JPMTR-2204
DOI 10.14622/JPMTR-2204
UDC 676.8|7.022-022.4|51-3

Original scientific paper | 164
Received: 2022-03-22
Accepted: 2022-07-15

Heightmap-based computing of the tool gap for additive manufacturing of paper embossing tools

Jakob Feldmann[1], *Dieter Spiehl*[1], *Edgar Dörsam*[1] *and Andreas Blaeser*[2]

[1]Technical University of Darmstadt,
Department of Mechanical and Process Engineering,
Institute of Printing Science and Technology,
Magdalenenstr. 2, 64289 Darmstadt, Germany
feldmann@idd.tu-darmstadt.de
spiehl@idd.tu-darmstadt.de
doersam@idd.tu-darmstadt.de

[2]Technical University of Darmstadt,
Department of Mechanical and Process Engineering,
Institute for BioMedical Printing Technology,
Magdalenenstr. 2, 64289 Darmstadt, Germany
blaeser@idd.tu-darmstadt.de

Abstract

Tools used for embossing paper and cardboard usually consist of two dies, which are inverses of each other. An important design parameter is represented by a defined gap between the fully closed dies. This is achieved by creating one of the two dies with an embossing relief that is displaced by a constant surface-normal offset. To facilitate fast data preparation for additive manufacturing of such embossing tools, a heightmap-based image data processing is developed, although the preparatory steps and resulting data may be also used for conventional manufacturing. The fundamentals of paper embossing tool layout and relief representation in heightmap images are explained and the developed process steps and their calculation bases are discussed. The focus is placed on the derivation of a heightmap with constant normal offset with respect to an input heightmap. For this purpose, image processing algorithms are elucidated to first determine the relief's surface curvature and use this information to deduce the necessary alteration to receive a derived heightmap. The generated data is reviewed and evaluated regarding its suitability for the production of additively manufactured embossing tools, which is done by examining the data as well as the derived physical dies.

Keywords: 3D printing, stereolithography, image processing, heightmaps, direct tooling

1. Introduction and background

In addition to printed texts, logos and images, embossments are used as a high-quality finish of paper, packaging and cardboard products. They do not only enable a visible change of the substrate's surface, but also add a haptic component to its design. Handling the print product, the customer can feel the embossment supporting the impression of a brand logo, writing or other features. For this reason, embossed details can be found on packages of products for the end consumer market as well as on business cards and other print media, where a high-quality finish is desired. Whereas for graphical print digital options exist, such as inkjet printing, which make them suitable for one-off and small-scale production, embossments can only be achieved with aid of embossing tools, which have to be produced for each embossment design individually (Iggesund, 2009, pp. 29–31). High cost and time consumption of the production of these tools can make them virtually unsuitable for individual or small-scale production of paper and cardboard products or make these very expensive to acquire. As shown in Figure 1, embossing tools for blind embossing consist of two halves, a female and a male die. The male die depicts the inversion of the female die and is used to drive the substrate into the desired shape by pushing it into the female die under the application of pressure (Iggesund, 2009).

In conventional manufacturing, embossing tools are often made from metals. Brass and steel tools are machined by a high resolution CNC or an engraving process (Fachverband deutscher Stanzformhersteller e.V., n.d.). Tools made of copper or magnesium can

also be created using etching processes. In contrast to metal cutting, etching processes are more cost-effective, but also limited in the achievable relief geometry of the embossing tools. Embossed reliefs, which are created by etching, usually consist of only two levels, while detailed height gradations and transitions can be achieved by milling or engraving. Further, embossing tools made of copper or magnesium are much less durable than ones machined from brass or steel (Iggesund, 2009, pp. 29–31). Depending on the paper thickness (caliper) of the intended substrate, the geometry of one of the two dies needs to be offset from the other in order to create a gap between the fully closed tool halves (Iggesund, 2009; Kirwan, 2013).

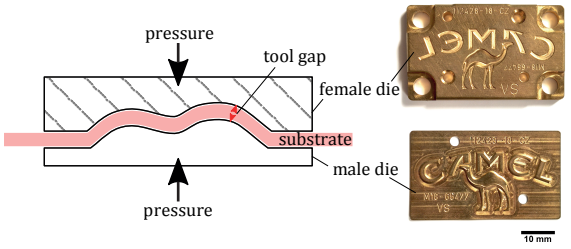

Figure 1: Schematic sectional view of a closed embossing tool with inserted substrate and an example of a conventional embossing tool made of brass

As an alternative to machining or etching both dies, the female die can also be used as a mold to cast the male die with e.g. thermoset resins. However, this approach holds a challenge. Casting of the male geometry does not allow for a large tool gap, as the only means of creating an offset between the two dies is through planned shrinkage of the thermoset resin during curing. Further, the shrinkage of the resin is hardly controllable, as it depends on the used materials, temperatures and geometries of the relief. Higher shrinkage, which is needed for thicker cardboard materials, also leads to higher residual stresses in the material and induces undesired warping (Zarrelli, Skordos and Partridge, 2002), further limiting the gap achievable using this method. A constant and defined tool gap is desirable as it allows for cleaner embossments and easier handling.

Delić, et al. (2017) investigated the suitability of additive manufacturing processes for the production of simple paper embossing tools. Therein, the Fused Filament Fabrication (FFF) process is used to fabricate two-part embossing tools. The authors conclude that, in principle, functional embossing tools can be created using this approach, but that deficiencies occur with embossing reliefs that are rich in detail and complex. Especially with increased fabrication speed, FFF produced tools show limitations in the reproduction of small elements often included in paper and cardboard embossments (Žarko, et al., 2017). However, the studies on FFF printed embossing dies show the need for a rapid tooling solution for paper embossing dies. Rapid tooling describes the additive manufacturing of tools as patterns or molds of a final part. It intends a fast and effective production launch rather than a high quantity of produced goods (Gibson, Rosen and Stucker, 2015).

Feldmann, Spiehl and Dörsam (2021) are presenting a novel approach for the production of paper embossing tools using heightmap data and masked stereolithography based additive manufacturing (MSLA). The process was shown to reduce manufacturing lead times from a full business day to approximately 2.5 hours. The MSLA can be classified as one of the additive manufacturing processes with the highest part resolution (Kim and Oh, 2008) and surface qualities (Li, et al., 2017) and has therefore proven to be a suitable manufacturing process for tools for paper embossing with a high level of detail and smooth surfaces. The presented approach allows for a cost-efficient manufacturing of prototype tools as well as for small to mid-scale production of embossed media of up to 20 000 pieces (Feldmann, Spiehl and Dörsam, 2021).

The present study focuses on the relief surface-normal tool gap, which is created by an offset of the male from the female relief. It centers on the preparation process for the computation of this gap in the geometry data, with the aim of using MSLA additive manufacturing for the tool fabrication, and evaluates the thereby created embossing tools. In the tool design a secondary gap between both fully closed die blocks outside of the relief geometry is also considered. This secondary gap is larger than the intended substrate's thickness in order to not compress and deform it where not desired. It is achieved by an additional elevation of the male relief from the die block's surface. In Figure 2 the functional features of embossing dies are shown in a schematic cross-sectional view of a closed tool.

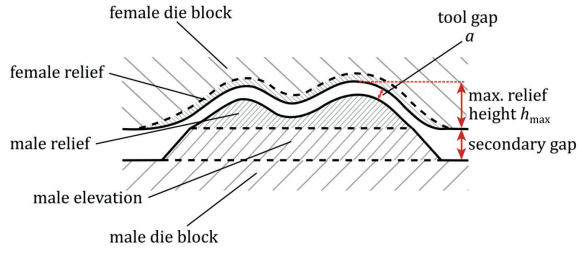

Figure 2: Diagram of the functional features of a paper embossing tool; a distinction is made between a tool gap a in the area of the embossing relief and a secondary gap outside the deformation area that serves the purpose to leave room for the substrate where it must not be deformed; the maximum relief height h_{max} is highlighted

2. Materials and methods

2.1 Heightmap images for representation of embossment reliefs

Heightmap (also *heightfield* or *displacement map*) images are usually 8-bit grayscale raster images first used by Cook (1984) to represent relief data for digital application such as rendering. Due to their small data size heightmaps are used as an efficient method to define surface data and can easily be viewed, edited and used in conventional image editors as well as transformed for use in 3D programs. A set gray value for each pixel defines the elevation of this point out of the base surface (Karhu, 2002). Using 8-bit grayscale images, elevations in a resolution of $2^8 = 256$ steps are achievable. Following Doggett (2001), conventionally, values of 0 (fully black) represent no elevation, while 255 (fully white) represent the highest points of the surface.

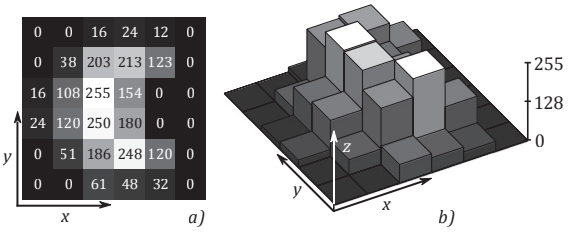

Figure 3: Exemplary illustration of a 6 × 6 pixel heightmap: elevation values are depicted as grayscale shades as well as values from 0 to 255 in (a); part (b) displays a three-dimensional representation, where pixels are raised from the image plane according to their elevation values

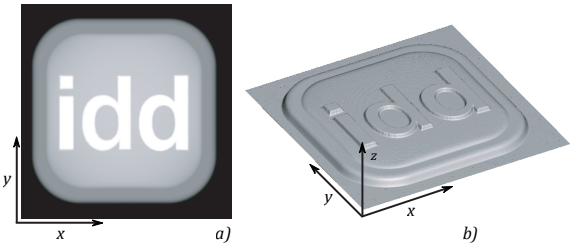

Figure 4: Comparison of an 8-bit heightmap (737 × 749 pixels, x × y) in (a), with the rendered relief derived from it (b): elevation of each point on the heightmap is represented by the brightness of the corresponding pixel; the representation of (b) is smoothed via a triangulation over the pixel values

Figure 3 shows a schematic diagram of a 6 × 6 pixel heightmap and Figure 4 displays the relief geometry of an embossment as a heightmap and as a rendered three-dimensional representation. Heightmap images are dimensionless. In order to use them for depictions of real objects, the dimensions of the image plane and the step height of the gray levels must be specified. As for each pixel on the image plane only one elevation value can be defined, heightmaps are unable to display overhangs and undercuts and are limited to surface curvature angles up to 90°. Further, due to the discretization in 256 steps, the resolution might not be sufficient in applications with shallow slopes or high elevations, as steps could be visible in the three-dimensional relief.

For the definition of embossing geometries, heightmaps are commonly used for the communication between designer and manufacturer. This is primarily the case for complex, three-dimensional designs, where elevation cannot be derived easily from 2D vector images. The aforementioned limitations in the application of heightmaps do not pose a problem for the definition of embossments, as the embossing of paper and cardboard share the same restrictions, such as the maximum surface curvature angle and the inability to display undercuts. Limits of the elevation resolution also play a subordinate role, as embossing features are usually rather flat reliefs with minor elevations of usually less than 1 mm, where 256 discrete steps serve sufficiently enough to display smooth transitions and details. Further, manufacturing methods generally pose more severe limitations in elevation resolution, which reduces the necessity for higher resolution in the images even more.

2.2 Image processing for tool gap

As mentioned before, an important design parameter in the layout of embossing tools is the gap between the reliefs of the closed female and male dies. It is desirable to manufacture corresponding dies with a uniform gap between both reliefs, which is of constant thickness along the curvature of the surface. In order to achieve such a tool gap, an image processing algorithm was developed, which can compute a fitting male relief heightmap with a predefined offset from a given female original heightmap or vice versa.

We set the originally designed heightmap to represent the relief towards the viewer and calculate either a shrunk male heightmap for an embossment, where the relief is raised out of the image plane, or an enlarged female heightmap for a debossment, where the relief is lowered into the image plane, for the die for the back side. Image processing, rather than 3D modelling, was utilized to decrease calculation time by reducing overall complexity of the calculation. For the sake of simplicity this publication will first discuss the calculation of a male heightmap-based on a female heightmap. Following, the few differences to the reverse process will be outlined. The developed image processing

algorithm was realized in *Python 3.*7 using the *NumPy* library (NumPy community, 2020). We need to define the dimensions of the desired embossing relief before commencing the image processing. Therefore, the physical image width of the heightmap, maximum relief height h_{max} and tool gap a (see Figure 1) need to be specified beforehand.

In a first step, the surface curvature at each point of the original heightmap is calculated, which is necessary to determine the surface-normal needed for the tool gap. For this a minimum filter oriented approach was used. Pixel wise the value of each pixel of the original heightmap $H_{orig,i,j}$ is compared to all other pixel values within a predefined kernel size around it. Larger kernel sizes result in smoother surfaces, albeit tending to blur details. Although the kernel size can be chosen arbitrary, we received best results with reasonable computing times when setting a kernel with a side length of approximately twice the desired tool gap. The distance $s_{i,j}$ between the kernel center pixel and the pixel with the lowest value within the kernel area is calculated (Figure 5a). If two or more pixels with equal values are found to be the lowest within the kernel area, the lowest distance between the center and one of these is considered to be $s_{i,j}$ (Figure 5b). In the case the center pixel itself has the lowest value within the area, or if all pixels within the area share the same value, the distance $s_{i,j}$ is considered to be zero (Figure 5c). All three cases are shown in Figure 5.

Further, we also determine the difference in pixel value $d_{i,j}$ between the pixel under consideration and the calculated lowest pixel in the kernel area. Again, if either the center pixel is the lowest or all pixels share the same value, the difference $d_{i,j}$ is considered to be zero.

With aid of the now known values $s_{i,j}$ and $d_{i,j}$ for each pixel, we can compute the local curvature $\theta_{i,j}$ through a trigonometric equation. Figure 6 shows a schematic representation of values needed for the determination of the curvature angle. A simplified diagram visualizing the calculation of the local curvature angle can also be seen in step 1 of Figure 8. As heightmaps represent dimensionless reliefs, we need to incorporate the real pixel size d_{px} and gray value step height h_{step}, which is calculated from the maximum relief height h_{max} divided by 255, to receive the curvature of the real surface:

$$\tan(\theta_{i,j}) = \frac{d_{i,j}}{s_{i,j}} \cdot \frac{h_{step}}{d_{px}} \quad [1]$$

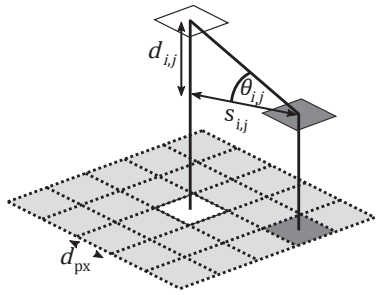

Figure 6: Schematic representation of value difference d between center and lowest pixel and pixel distance s between center and lowest pixel in a 5 × 5 kernel; curvature angle θ is calculated using a simple trigonometric equation

As an example, Figure 7 shows a plot of the surface curvature angle of the heightmap given in Figure 4. Values were calculated for each image pixel *i,j* following the above-mentioned method and Equation [1]. The maximum height of the relief h_{max} was set to 1 mm resulting in a step height of $h_{step} \approx 3.92$ µm and the image width to 50 mm resulting in a pixel size of $d_{px} \approx 67.84$ µm.

In a second processing step, the pixel grayscale values of the matching male heightmap need to be determined. In order to receive the male heightmap, the value of each pixel of the original heightmap needs to be reduced by the correct z-offset $\delta_{i,j}$ to result in the predefined surface-normal tool gap a.

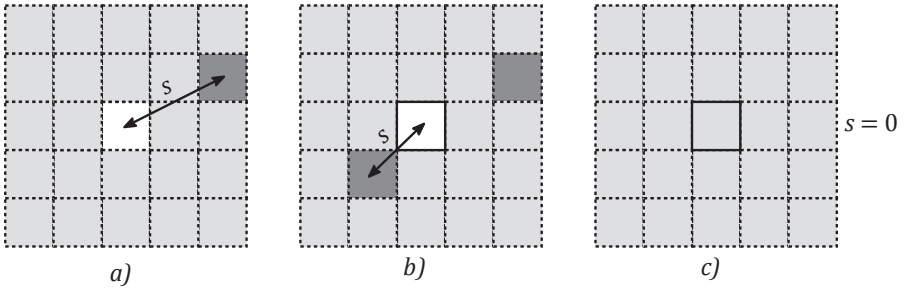

Figure 5: Schematic representation of the three cases for calculating the distance s with a 5 × 5 kernel, which is propagated for each pixel of the original heightmap image: (a) the distance s is considered to be the distance between the center pixel and the lowest (darkest) pixel of the kernel area, (b) if more than one pixel with the lowest value exists within the kernel area, the distance to the closest pixel from the center is considered, (c) if all pixels within the kernel area share the same value, the distance is considered to be zero

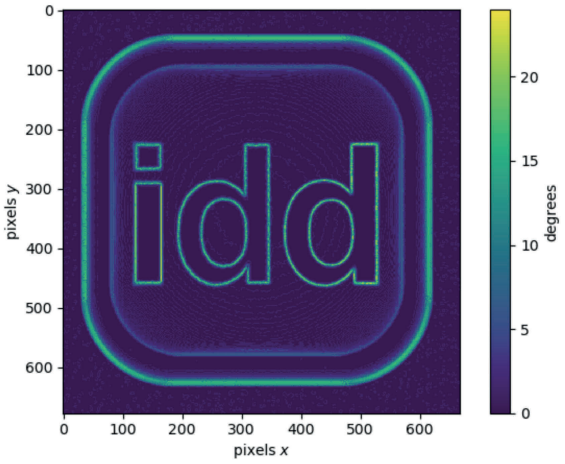

Figure 7: Calculated surface curvature of heightmap shown in Figure 4

The amount each pixel value needs to be reduced by was therefore calculated with a second trigonometric equation and the local surface curvature angle $\theta_{i,j}$ calculated by Equation [1]. Here we needed to incorporate the step height again in order to receive a value for the z-offset $\delta_{i,j}$ in dimensionless grayscale.

$$\delta_{i,j} = \left\lfloor \frac{a}{\cos(\theta_{i,j})} \cdot \frac{1}{h_{\text{step}}} \right\rfloor, \quad \delta_{i,j} \in \mathbb{Z} \qquad [2]$$

Because 8-bit heightmaps are limited to integer numbers, $\delta_{i,j}$ was rounded down by the floor function. Figure 8 shows a summary of the two processing steps in a two-dimensional representation.

As a third and final step, the male heightmap was achieved by subtracting the local value of $\delta_{i,j}$ from each pixel of the original heightmap. Where the result would be negative it was set to zero.

$$H_{\text{male},i,j} = \begin{cases} H_{\text{orig},i,j} - \delta_{i,j}, & (H_{\text{orig},i,j} - \delta_{i,j}) \geq 0 \\ 0, & (H_{\text{orig},i,j} - \delta_{i,j}) < 0 \end{cases} \qquad [3]$$

If the above-mentioned reverse process is required to create a female heightmap from a male original, a few changes must be considered.

The local surface curvature angle $\theta_{i,j}$ and the required z-offset for each pixel $\delta_{i,j}$ can be determined in the same way as shown in Equations [1] and [2] earlier. When adding $\delta_{i,j}$ to the original heightmap rather than subtracting it, we can enquire values which exceed 255, which is the largest value 8-bit grayscale is defined for. In order to avoid this problem, we reduced the original heightmap by a factor k. The largest possible value for $\delta_{i,j}$ is a/h_{step}, hence we choose

$$k = \frac{255}{255 + \frac{a}{h_{\text{step}}}} \qquad [4]$$

in order to preserve the maximum possible resolution for the resulting female heightmap, without exceeding values of 255. A female heightmap can then be calculated by adding the z-offset $\delta_{i,j}$ to the original heightmap and multiplying the result by the factor k. Values of the female heightmap were rounded to the nearest integer number.

$$H_{\text{female},i,j} = \lfloor k(H_{\text{orig},i,j} + \delta_{i,j}) + 0.5 \rfloor, \quad H_{\text{female},i,j} \in \mathbb{N}_0 \qquad [5]$$

2.3 Layer images from heightmap data

The MSLA and comparable additive manufacturing requires raster layer images (or *layer masks*), where all parts of the layer, which should be exposed to light and therefore solidified, are shown as white while all others are shown as black pixels. To receive respective layer images from previously computed heightmaps, a simple threshold function can be utilized, which incorporates each heightmap pixel value and considers layer number l as well as dimensional step h_{step} and

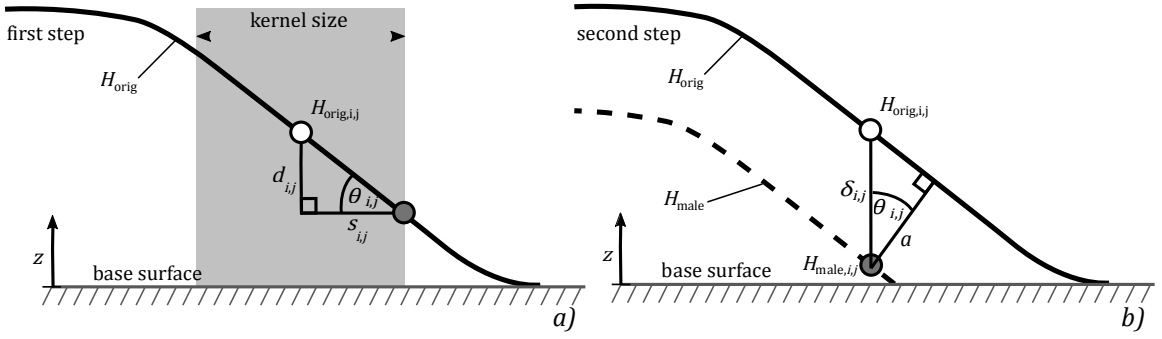

Figure 8: Graphical two-dimensional representation of the two subsequent computing steps for the calculation of the offset male heightmap H_{male}: in the first step (a), the lowest value inside the kernel size around each point on the original heightmap allows for the calculation of the surface curvature; in the second step (b), the value by which the male heightmap needs to be offset in z-direction is calculated to achieve a constant surface-normal tool gap of a

layer heights h_{layer}. The layer number l is increased by 1 for each new layer of image until the whole relief is processed. Thus, we set layer image pixels $L_{i,j}$ to either white (255) or black (0) under the following conditions, where k = 1, if not specified differently before:

$$L_{i,j} = \begin{cases} 0, & H_{i,j} < l \cdot k \cdot \dfrac{h_{layer}}{h_{step}} \\ 255, & H_{i,j} \geq l \cdot k \cdot \dfrac{h_{layer}}{h_{step}} \end{cases} \quad [6]$$

$H_{i,j}$ may be $H_{orig,i,j}$, $H_{male,i,j}$ or $H_{female,i,j}$ depending on which geometry was created. Figure 9 shows a schematic of how one respective layer image is calculated following the threshold function in Equation [6].

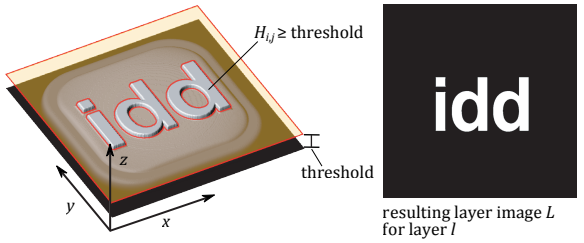

a) *b)*

Figure 9: Schematic visualization of the threshold algorithm for the derivation of layer images from a heightmap image: (a) the layer height is shown in opaque orange and all pixels that have a value greater than that of the respective layer threshold are kept and set to white (255), all others are set to black (0), (b) the resulting layer image

2.4 Evaluation methods

The data and results generated in the course of this research were evaluated using two methods. Firstly, the digital heightmap data obtained, which serves as the relief data basis for slicing and additive manufacturing, was examined. For this purpose, the derived heightmap's surface curvature and surface-normal tool gap to the original heightmap was calculated in analogy to the image processing algorithm described earlier. Further, a cross sectional view of both dies can be visualized by plotting the elevations of both reliefs along a defined path on the heightmap. Taking the real pixel size d_{px} and gray value step heights h_{step} into consideration the dimensions of the expected dies can be displayed.

Secondly, next to the raw data used for the generation of the layer images, the real MSLA additively manufactured tool was scanned using an optical 3D profilometer (*Keyence VR 5200*, Keyence, Japan) with an optical magnification of 12 times which results in a lateral resolution of 23.53 µm. Additive manufacturing was realized on an MSLA machine (*Zortrax Inkspire*, Zortrax, Poland) with a pixel resolution of 1 440 × 2 560 and a display size of 74.67 mm × 132.88 mm, which results in a pixel size of approximately 50 µm. The layer height was set to the minimum of 25 µm, recommended by the manufacturer. For easier measurement of the male relief elevation, the secondary gap (see Figure 2) was set to zero, in order to use the male block's top surface as a reference.

3. Results and discussion

Heightmap data created with the presented image processing workflow was successfully used for the manufacturing of fully functional additively manufactured embossing tools. Derived from a single original heightmap, corresponding reliefs for female and male tool dies could be obtained, depending on whether an embossment or debossment is desired. Figure 10 shows resulting shrunk male and enlarged female heightmaps fitting to a given original heightmap.

As the male heightmap uses the same z-scale as the original, and therefore the same step height h_{step}, it appears darker as it is reduced in elevation. Further, raised (brighter) areas appear thinner, while lower (darker) parts are broader to allow for a constant offset between original and calculated male relief. As described in section 2.2, enlarged female heightmaps are set to a new z-scale and therefore do not appear brighter, but broader raised areas as well as thinner sunken parts can be identified visually. The developed process allows for a quick design of relief data. Existing images of logos and emblems can easily be transferred into grayscale heightmaps in common graphic editing software, e.g. *GIMP* (GIMP Development Team, 2022), where an editor chooses different shades of gray for different elevation levels and brightness gradients for slopes. We differentiate between embossments, where the substrate is convexly raised towards the viewer, and debossments, where the substrate is concavely recessed by the tool. As mentioned before, we set the original heightmap to represent the relief towards the viewer and compute either a shrunk male heightmap (embossment) or an enlarged female heightmap (debossment) for the die of the back side. This also allows for the same design to be applied to different cardboard types and thicknesses. While the relief towards the viewer may remain unaltered, the die serving as an inverse for the back side can be adapted according to the requirements of the used substrate and the embossing process.

Figure 11 shows a partial cross section view of the data sets of an original heightmap and a computed offset, hence shrunk, male heightmap to realize an embossment. In the example the female relief depth h_{max} was

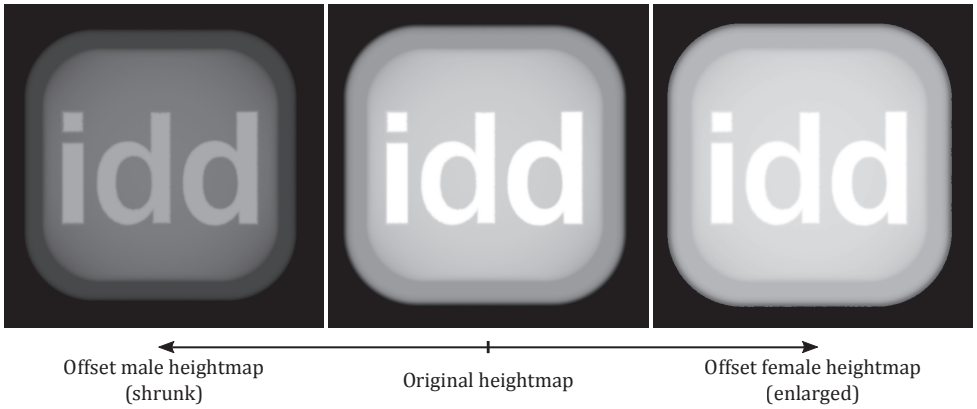

Figure 10: View of the original heightmap as well as the shrunk male and enlarged female heightmap derived from it; we choose the original to represent the relief towards the viewer and calculate either a male heightmap for an embossment or a female heightmap for a debossment for the die for the back side

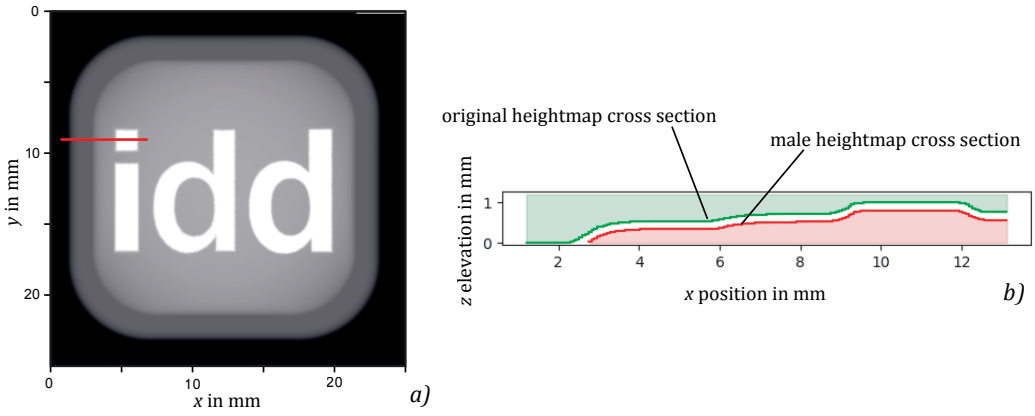

Figure 11: Cross section view of the heightmap data elevation profile along the path represented by the red line in part (a) of the figure, the profiles of original (green) and calculated male heightmap (red) are depicted in part (b)

set to 1 mm and the tool gap was chosen to be 0.1 mm. Elevation and distances in the *x*-*y*-plane were converted into unit quantities using h_{step} and d_{px}. It can be seen that a constant tool gap between both reliefs was successfully achieved with the calculated male heightmap closely following the curvature of the original heightmap, regardless of its slope angle and direction.

The error of the computed tool gap was found to be within 7 µm for a preset value of 0.1 mm for *a* and the largest deviations were identified in areas of higher surface curvatures, as can be seen in Figure 12. This implies that the approximation is error-prone in the region of large values for the quotient of $d_{i,j}$ and $s_{i,j}$. Since the technically relevant minimum resolution of additive manufacturing systems in question is in the order of 25 µm, such expected deviations of the tool gap are only of minor importance and can be accepted as sufficiently precise. Such resolutions were found to be sufficient for the intended use case for paper and cardboard embossing, as the layer pattern resulting from the stair casing effect in additive manufacturing could not be identified with the unaided eye (Feldmann, Spiehl and Dörsam, 2021).

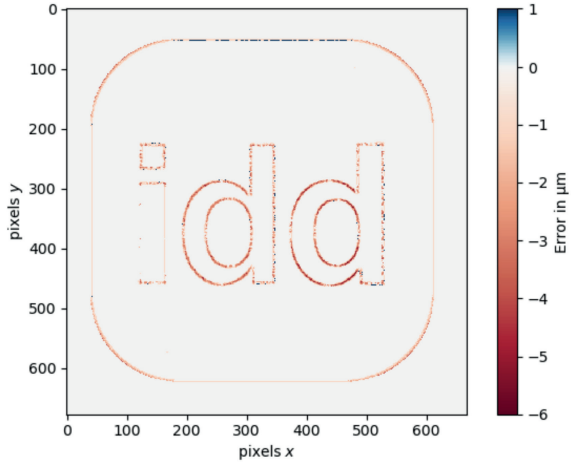

Figure 12: Plot of local tool gap deviation from the desired preset value of a = 0.1 mm between original and male heightmap data

The tool dies were set to the aforementioned dimensions (1 mm depth, 50 mm image width and 0.1 mm tool gap), in addition a secondary gap of 0.7 mm was chosen to not compress the paper where not intended and a rough paper with a grammage of 150 g/m^2 was embossed with 15 kN force.

When examining the additively manufactured embossing dies, which were fabricated based on the calculated data, it can be demonstrated that the set tool gap is also carried over onto the physical tool. A scan of the tool surface via 3D optical profilometry is shown in Figure 13. Although the tool gap is present over the whole layout of the relief and is especially very uniform as well as of the desired thickness of 0.1 mm in even and flat areas, larger deviations than in the heightmap data mentioned before can be found at high surface curvatures, where the surface-normal tool gap was found to be up to 0.14 mm. These can be explained by the coarser resolution of the used additive manufacturing system, which becomes particularly apparent in the area of gradients. While the defined female relief height h_{max} of 1 mm could be depicted in 255 discrete steps in the heightmap, in the physical tool it is created with only 40 layers of 25 µm height. Furthermore, inaccuracies in the building process as well as handling can cause rounding along sharp edges, which can be seen along the rim of the female relief in the cross-section view of Figure 13. However, deviations were found to be small enough to not cause major deficiencies in the embossing process or in the embossing results. An embossment created using an embossing tool designed and manufactured in the here described process is shown in Figure 14.

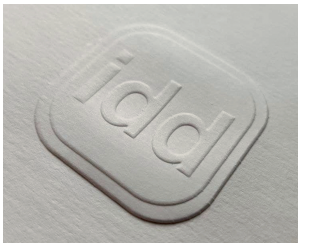

Figure 14: Embossing result in rough paper of 150 g/m^2 grammage by an additively manufactured embossing tool of 1 mm depth with a 0.1 mm tool gap, a force of 15 kN was applied to emboss the substrate; the embossment has a size of 38 mm × 38 mm

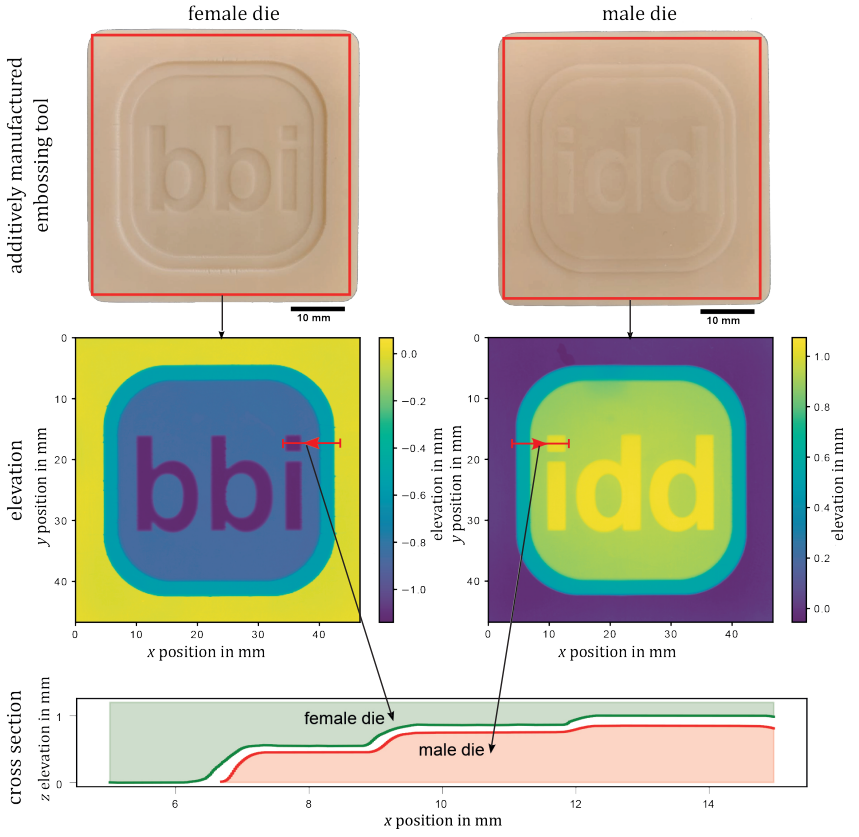

Figure 13: Display of a relief analysis of the additively manufactured embossing tool; 3D scans of the relief surfaces of both dies were realized using an optical profilometer, the figure shows images of the manufactured female and male embossing die, where the area of the scan is highlighted in red; the scanned surface elevation as well as a cross section view of the closed dies are displayed below

4. Conclusions and outlook

The investigation shows that heightmap data is suited for direct processing into layer images for additive manufacturing of embossing tools without the need for other preparatory 3D modelling software. Embossing reliefs can be derived from images used for graphic print and can therefore be easily and quickly processed in the same work environment. The method, thus, has the potential not only to reduce the production time of embossing tools, but also to enable faster provision of processable data. It was further shown, that the relief of a complementary die of a two-part tool with a defined surface-normal offset can be calculated using the presented algorithm. The derived complementary die exhibited minor deviations from the desired size (< 7 µm), which is smaller than the resolution of conventional additive manufacturing technologies and thus neglectable. A 3D surface scan of the additively manufactured tool showed that the largest deviations arise from the manufacturing process rather than from the data preparation, which could possibly be reduced by choosing an MSLA system with a higher resolution and further improvement of the setup and workflow. Nevertheless, these deviations are small enough to not cause deficiencies in the embossing process or result.

Experience shows that during embossing the substrate experiences particularly high stresses in areas that exhibit high degrees of deformation. These are prone to result in failures of the embossment. Therefore, determining these areas of high degrees of deformation based on the surface curvature angle and dynamic adjustment of the tool gap could be possible content of future research. This could distribute loads more evenly over the substrate and reduce stress peaks, which would potentially have a positive effect on process reliability and the achievable maximum embossing depth. Finally, 3D scanning of the embossing result on the substrate and comparison with the original heightmap data could allow for a regulated adjustment of the relief data and tool gap. It could also provide a deeper understanding of the embossing deviations in comparison to the original data, which may allow general rules on embossing transfer to be derived.

Future work is therefore aimed at the estimation of an embossing result based on gathered information gained from a comparison between the original heightmap and the 3D scanned embossing result. This could potentially not only reduce production times per iteration, but reduce the necessity for iterations and trial embossings overall.

Acknowledgments

We kindly acknowledge the support by *Zentrales Innovationsprogramm Mittelstand* (ZIM), grant number 16KN084522, of the German Federal Ministry for Economic Affairs and Energy (BMWi).

References

Cook, R.L., 1984. Shade trees. *Computer Graphics*, 18(3), pp. 223–231.

Delić, G., Vladić, G., Pál, M., Banjanin, B. and Dedijer, S., 2017. *Performance evaluation of paper embossing tools produced by fused deposition modelling additive manufacturing technology*. *Journal of Graphic Engineering and Design*, 8(2), pp. 47–54. http://dx.doi.org/10.24867/JGED-2017-2-047.

Doggett, M.C., 2001. *Displacement mapping and volume rendering graphics hardware*. Habilitation dissertation. Universität Tübingen, Germany.

Fachverband deutscher Stanzformhersteller e.V., n.d. *ESUpedia: Stanzwerkzeuge für die Karton- und Wellpappenverarbeitung*. Meerbusch, Germany: Europäische Stanzform Union e.V.

Feldmann, J., Spiehl, D. and Dörsam, E., 2021. *Paper embossing tools: a fast fabrication workflow using image processing and stereolithography additive manufacturing*. In: C. Ridgway, ed. *Advances in Printing and Media Technology: Proceedings of the 47th research conference of iarigai*. Athens, Greece, 19–23 September 2021. Darmstadt: iarigai, pp. 146–154. http://dx.doi.org/10.14622/Advances_47_2021.

Gibson, I., Rosen, D. and Stucker, B., 2015. *Additive manufacturing technologies: 3D printing, rapid prototyping, and direct digital manufacturing*. 2nd ed. New York, NY: Springer.

GIMP Development Team, 2022. *GIMP: GNU image manipulation program.* [computer program] Available at: <https://www.gimp.org> [Accessed March 2022].

Iggesund Paperboard AB, 2009. *Graphics handbook – paperboard the Iggesund way*. Solna, Sweden: Intellecta Infolog, Iggesund Paperboard AB.

Karhu, K., 2002. Displacement Mapping. In: *Helsinki University of Technology, Tik–111.500 Seminar on computer graphics*. Helsinki, 2 April 2002.

Kim, G.D. and Oh, Y.T., 2008. A benchmark study on rapid prototyping processes and machines: quantitative comparisons of mechanical properties, accuracy, roughness, speed, and material cost. *Proceedings of the Institution of Mechanical Engineers, Part B: Journal of Engineering Manufacture*, 222(2), pp. 201–215. http://dx.doi.org/10.1243/09544054JEM724.

Kirwan, M.J. ed., 2013. *Handbook of paper and paperboard packaging technology*. 2nd ed. Chichester, UK: Wiley-Blackwell.

Li, Y., Linke, B.S., Voet, H., Falk, B., Schmitt, R. and Lam, M., 2017. Cost, sustainability and surface roughness quality – a comprehensive analysis of products made with personal 3D printers. *CIRP Journal of Manufacturing Science and Technology*, 16, pp. 1–11. http://dx.doi.org/10.1016/j.cirpj.2016.10.001.

NumPy community, 2020. *NumPy Reference*: *Release 1.18.1*. [online] Available at: <https://numpy.org/doc/1.18/numpy-ref.pdf> [Accessed March 2022].

Zarrelli, M., Skordos, A.A. and Partridge, I.K., 2002. Investigation of cure induced shrinkage in unreinforced epoxy resin. *Plastics, Rubber and Composites*, 31(9), pp. 377–384. http://dx.doi.org/10.1179/146580102225006350.

Žarko, J., Vladić, G., Pál, M. and Dedijer, S., 2017. Influence of printing speed on production of embossing tools using FDM 3D printing technology. *Journal of Graphic Engineering and Design*, 8(1), pp. 19–27. http://dx.doi.org/10.24867/JGED-2017-1-019.